Design of an Electro-Optic Polarization Switch for a High-Capacity High-Speed Digital Light Deflection System

BY S. K. KURTZ

(Manuscript received April 26, 1966)

Modulator requirements for an active electro-optic polarization switch to operate in a digital light deflector (DLD) are derived. It is shown that a simple capacity-speed product of the form (capacity)$^{\frac{1}{2}}$ × (address rate) ≦ (constant) × (driver power) can be derived for both linear and biased quadratic electro-optic modulator materials. The usefulness of this relation is demonstrated by applying it to a biased quadratic electro-optic material (KTN) and two linear electro-optic materials ($LiNbO_3$ and ZnTe).

The results indicate that KTN will operate a DLD at a rate of 10^6 random addresses/sec and a capacity of 10^6 addresses with a reactive power of 2.6 watts, a bias voltage of 1200 volts, and a driver voltage of 42 volts, provided,

(i) fluctuations in the Curie temperature and ambient operating temperature are held to less than 0.01°C,

(ii) some form of ac bias is used to circumvent space charge effects, and

(iii) strain and defect-free material meeting these requirements can be grown to a size of at least 1 × 1 × 2 cm.

A linear electro-optic material such as ZnTe with a reduced half-wave voltage (unity aspect ratio) in the 2 to 3-kV range (2.5 kV at 6000 Å) will provide 3.6 × 10^6 addresses at a rate of 10^6 addresses/sec with a reactive driver power of 10 watts, delivered at a drive voltage of 1250 volts.

Experimental results obtained using KTN as a high-speed pulsed light modulator are also presented.

I. INTRODUCTION

In this paper we examine the design of a high-speed optical polarization switch utilizing the electro-optic properties of certain crystalline solids. Primary emphasis has been placed on potassium tantalate-niobate, but linear electro-optic materials are also considered. The design

equations are applied to a switch for a 10^6 addresses/sec digital light deflector (DLD) described by Nelson[1] and Tabor.[2]

In Section II a derivation of the capacity-speed equation is given. Sections III and IV discuss the reactive power limitations due to heating of a KTN modulator, and typical operating characteristics for a high-speed modulator are tabulated. Section V discusses additional limitations on the capacity-speed product of KTN due to composition inhomogeneities and ambient temperature fluctuations. Space charge effects and ac biasing are treated in Section VI. In Section VII the advantages of a rectangular aperture are considered and a comparison is made of the capacity speed product of KTN with those of the linear electro-optic materials ZnTe and $LiNbO_3$. Finally, in Section VIII some experimental results are presented for pulse modulation of light using KTN.

II. DERIVATION OF THE CAPACITY-SPEED RELATION

A polarization switch in the DLD performs the function of "rotating" the plane of polarization of a light beam rapidly through 90°. The plane of polarization thus selected determines whether the beam traverses a Wollaston prism[2] as an ordinary or extraordinary ray (i.e., determines in which direction it is deflected). This is illustrated in Fig. 1 for one module (deflection unit) of the DLD. It is well known that such a 90° change in the direction of polarization of a light beam is produced by inserting a half-wave plate into a linearly polarized light beam with the preferred axes of the plate at a 45° angle with respect to the direction of polarization of the incoming light beam.

By substituting a crystal whose refractive indices can be varied electro-optically in place of the half-wave plate, we have an electrically variable phase retardation "plate." The desired "rotation" of 90° is achieved by applying an electric field to the crystal of the correct magnitude to produce a half-wave of phase retardation between the ordinary and extraordinary ray. This is illustrated in Fig. 2. It is obvious that for a given aperture A the total length of the DLD must be restricted for some upper limit in order to prevent the optical beam from "walking off" the aperture with consequent loss of intensity in the outermost positions of the beam. This, in turn, places an upper limit on the length of the individual modulation and deflection elements.

As originally described by Nelson[1] the DLD consists of an X deflection bank and an orthogonal Y deflection bank in series. Each bank consists of n modular units of varying length l_n, each module containing

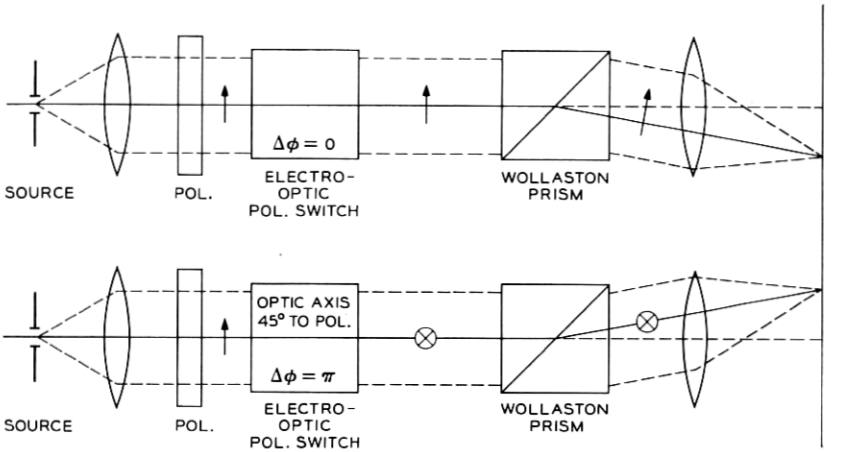

Fig. 1 — Operation of polarization switch in one deflection module of a DLD system.

an active polarization switch (modulator) and a passive birefringent deflector. The deflector thickness is predetermined to give a transverse linear displacement of the beam by distances which increase as multiples of 2, e.g., 2^0t, 2^1t_o, 2^2t_o, $2^3t_o \cdots 2^nt_o$. An improved version of the DLD described by Tabor[2] utilizes Wollaston prisms which give angular rather than linear transverse displacements. The thickness of the prisms is predetermined to give angular displacements $\pm 2^0\theta_o$, $\pm 2^1\theta_o$, $\pm 2^2\theta_o$, $\pm 2^3\theta_o \cdots \pm 2^n\theta_o$, resulting in a total of $2^n \equiv R$ angular positions in each dimension. In order that each of these angular positions be resolvable the basic angular unit of deflection $2\theta_o$ is chosen to be somewhat

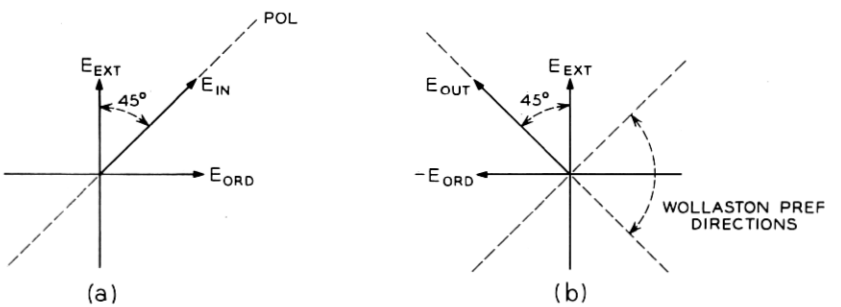

Fig. 2 — Retardation of plane of polarization by half-wave plate.

greater than the diffraction angle θ_D,

$$\theta_D = \frac{\lambda}{d} \tag{1}$$

where d is the width of the aperture.

It is convenient to define $\beta = (2\theta_o/\theta_D) > 1$. Assuming that the DLD consists of $2n$ modules of equal* length l_m, we order the modules serially in terms of increasing angular deflection.

$$\theta_{1x}, \theta_{1y}, \theta_{2x}, \theta_{2y}, \cdots, \theta_{nx}, \theta_{ny}. \tag{2}$$

This ordering minimizes walk-off since it puts the largest deflections closest to the exit part of the assembly. For this configuration the maximum cumulative walk-off (displacement at the exit part transverse to the axis of the DLD) is given by,

$$\Delta x = \frac{3}{2\sqrt{2}} \beta l_m \theta_D R \tag{3}$$

$$\Delta y = \frac{\beta l_m \theta_D R}{\sqrt{2}} \tag{4}$$

where the linear capacity R is defined as

$$2^n = R. \tag{5}$$

The deviation of (3) and (4) is given in Appendix A.

If we restrict the loss of intensity in the extreme positions to be less than 20 percent (i.e., $\Delta x, \Delta y \leqq 0.14d$) then from (3) and (4) we obtain the following restriction on the length to aperture ratio for the modulator,

$$\frac{l}{A} \leqq \frac{3}{20\beta\lambda R\left[1 + \left(\frac{l_m - l}{l_m}\right)\right]} \tag{6}$$

where $A = d^2$ and $l \cong l_m$.

The next step in the derivation is to show that for both linear transverse electro-optic materials and biased quadratic electro-optic materials the reactive power is proportional to the cross-sectional area divided by the modulator length.

When an electric field is applied along a crystallographic {100} axis the principal refractive indices of KTN become[3,4]

* While in principal the prism length varies as 2^n, in practice each prism unit is the same length, being made up of an optically isotropic support section and a thin birefringent section which varies in the prescribed fashion.

$$n_o \cong n - \frac{n^3}{2} g_{12} P_z^2$$
$$n_e \cong n - \frac{n^3}{2} g_{11} P_z^2 \tag{7}$$

hence,

$$\Delta n = n_o - n_e = \frac{n^3}{2} (g_{11} - g_{12}) P_z^2 \tag{8}$$

where P_z is the induced lattice polarization in the {100} direction produced by the electric field. Here n is the isotropic refractive index in zero field and the g_{ij} are the quadratic electro-optic coefficients. The phase retardation can thus be expressed as

$$\Delta\varphi = \frac{2\pi}{\lambda} aP^2 l \tag{9}$$

where $a \equiv n^3/2\ (g_{11} - g_{12})$, l is the length of the KTN crystal in the light direction, and the z subscript on P has been dropped for simplification. From (9) the polarization required to give the first half-wave of phase retardation ($\Delta\varphi = \pi$) is

$$P_\pi = \left(\frac{\lambda}{2al}\right)^{\frac{1}{2}}. \tag{10}$$

The quadratic dependence of phase retardation on lattice polarization leads to a successively closer spacing of half-wave points ($\Delta\varphi = m\pi$, m a positive integer) as shown in Fig. 3. If we define the dielectric permittivity at a bias polarization $P = P_b$ as

$$\epsilon_b = \left(\frac{\partial P}{\partial E}\right)_{P=P_b}, \tag{11}$$

then the incremental voltage $\Delta V_{\pi b}$ which will produce a change in retardation of one half-wave at this bias point P_b can be written

$$\Delta V_{\pi b} \cong \frac{\lambda}{4a}\left(\frac{d}{l}\right)\left(\frac{1}{P_b \epsilon_b}\right). \tag{12}$$

For a material which exhibits a linear transverse electro-optic effect[5,6,7] the induced birefringence can be expressed,

$$\Delta n = n^3 r \frac{V}{d} \tag{13}$$

where V is the voltage applied perpendicular to the light path, d is the

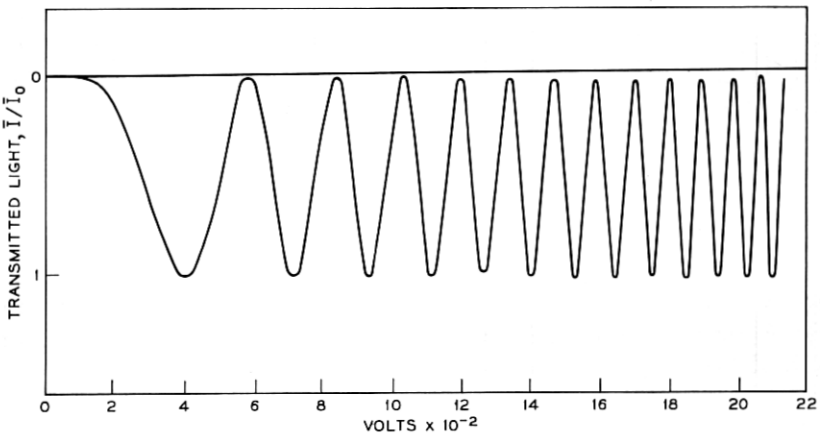

Fig. 3 — Light transmitted by KTN polarization switch as function of applied voltage.

electrode separation, and r is a function of the linear electro-optic coefficient(s) determined by the orientation of the crystallographic axes relative to the electric field and light directions.[4] The half-wave voltage V_π and reduced half-wave voltage v_π (for unity aspect ratio) can thus be defined from (13) as,

$$\Delta V_\pi = \frac{\lambda}{2n^3 r}\left(\frac{d}{l}\right) = v_\pi\left(\frac{d}{l}\right). \tag{14}$$

The reactive power delivered by the RF driver can be expressed* as

$$\mathcal{P}_r = \tfrac{1}{2}C(\Delta V_\pi)^2\nu_r = \alpha\left(\frac{bd}{l}\right)\nu_r \tag{15}$$

where

$$\alpha = \frac{\epsilon v_\pi^{\,2}}{2}, \tag{16}$$

for linear transverse electro-optic materials, and

$$\alpha = \frac{1}{2\epsilon_b}\left(\frac{\lambda}{4aP_b}\right)^2 \tag{17}$$

for biased quadratic electro-optic materials. An expression for α similar to (16) but valid for biased quadratic electro-optic materials is given in

* This is the case of a pulse train of the form 1,1,1,1,1, $\cdots$. A more complete discussion of the power is given in Appendix D.

Section VII (66). Substitution of (15) ($b = d$) into (6) yields the desired capacity-speed product for a square aperture modulator.

$$R\nu_r \leqq \Lambda \mathcal{P}_r \tag{18}$$

where

$$\Lambda = \frac{3}{20\alpha\beta\lambda\left[1 + \left(\frac{l_m - l}{l_m}\right)\right]}$$

and α is given in (16) and (17) for the linear transverse and biased quadratic cases, respectively, and we have assumed the term $(n + 1)/R$ is small compared to unity (for $n = 10$, $R = 1024$). The total capacity is of course R^2 and not R. The capacity-speed product is easily generalized to rectangular aperture (see Appendix B) with the results

$$(R_{x'}R_{y'})^{\frac{1}{2}}\nu_r \leqq \Lambda_{x'y'}\mathcal{P}_r \tag{19}$$

where

$$\Lambda_{x'y'} = \frac{1}{5\alpha\sqrt{\beta_x\beta_y}\lambda\left[1 + \frac{l_m - l}{l_m}\right]}\sqrt{\frac{2d}{b}}. \tag{20}$$

Let us consider the implications of the capacity-speed relation for a system with a square aperture. If the dielectric constant and reduced half-wave voltage of a linear electro-optic material are fixed constants, and the address rate ν_r is also fixed by the application to be made of the DLD, then the total capacity R_xR_y varies directly as the square of power available to drive the modulator. Conversely, if the capacity is fixed, the address rate varies linearly with the available power. The constant of proportionality Λ can be calculated for a given electro-optic material and hence the capacity-speed product becomes an important design equation for determining which materials can meet the capacity-speed product required in a specific application of the DLD. It also provides a significant comparison between linear and biased quadratic electro-optic performance. The remaining sections of this paper are concerned with evaluating the optimum capacity-speed product which can be obtained using KTN, and comparing this with the capacity-speed product obtainable using known linear transverse electro-optic materials. It is clear from the form of the capacity-speed product that the question which must be answered in both cases is: What are the limitations on the power with which the modulator can be driven?

III. DRIVER POWER LIMITATIONS FOR KTN

The purpose of a bias polarization P_b is to reduce the half-wave voltage V_π required to produce the 90° rotation of the light polarization. This is evident if we compare the unbiased half-wave voltage,

$$V_\pi = \left[\left(\frac{\lambda}{2a}\right)^{\frac{1}{2}} \frac{1}{\epsilon}\right]\left(\frac{d}{l^{\frac{1}{2}}}\right) \tag{21}$$

with the biased half-wave voltage in (12), and substitute P_π from (10) to obtain the following relation between biased and unbiased half-wave voltage,

$$\Delta V_{\pi b} = \frac{1}{2}\left(\frac{P_\pi}{P_b}\right) V_\pi \,. \tag{22}$$

The biased half-wave voltage therefore, decreases as the inverse of the bias polarization. It is helpful conceptually to express the bias polarization P_b in terms of the equivalent number of half-waves of retardation m it produces. Since the phase retardation (see (9)) varies as the square of polarization we can write

$$P_b = \sqrt{m}\, P_\pi \tag{23}$$

hence,

$$\Delta V_{\pi b} \cong \frac{1}{2\sqrt{m}}\, V_\pi \,. \tag{24}$$

The introduction of a bias polarization P_b can thus be used to reduce the drive voltage needed for the switch. Because of saturation effects in the induced polarization it is necessary at this point to differentiate between the low field permittivity ϵ and the small signal permittivity ϵ_b about the bias point P_b. Saturation behavior of KTN is describable in terms of the Devonshire free energy formalism.[8] Writing the free energy, as,

$$G = \left(\frac{T - T_o}{2\epsilon_o C}\right) P^2 + \frac{\xi}{4} P^4 + \frac{\zeta}{6} P^6 \cdots \tag{25}$$

we obtain,

$$E = \frac{\partial G}{\partial P} = \left(\frac{T - T_o}{\epsilon_o C}\right) P + \xi P^3 + \zeta P^5 \cdots \,. \tag{26}$$

Some useful relations which follow from (25) and (26) are given in Appendix C.

A plot of (26) illustrating saturation effects along with some experimentally measured points is shown in Fig. 4. In Fig. 5 we have plotted

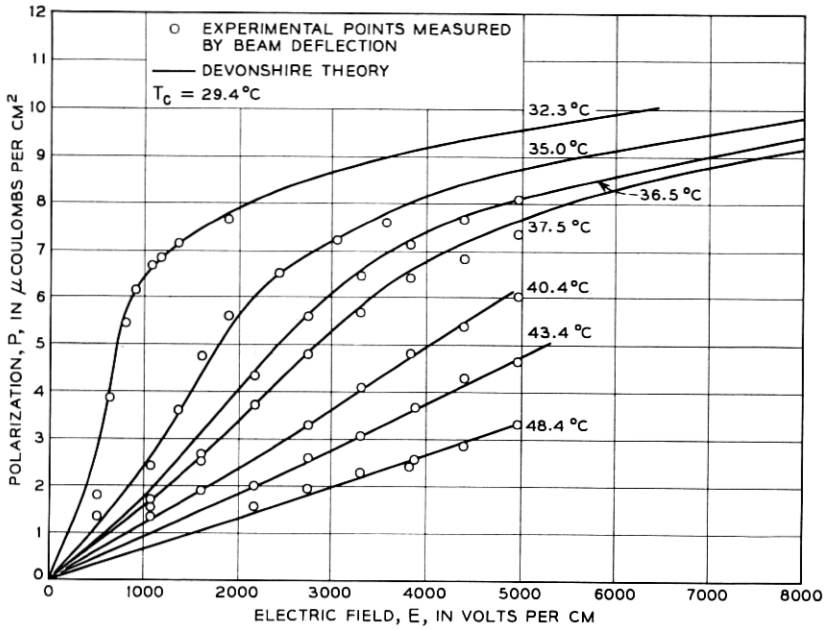

Fig. 4 — Saturation effects in the induced polarization of KTN as a function of temperature.

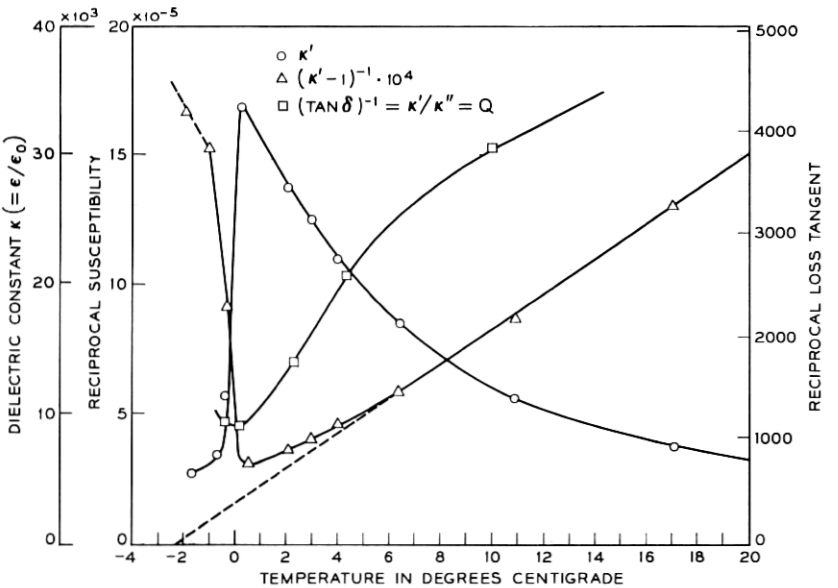

Fig. 5 — Dielectric behavior of KTN as a function of temperature.

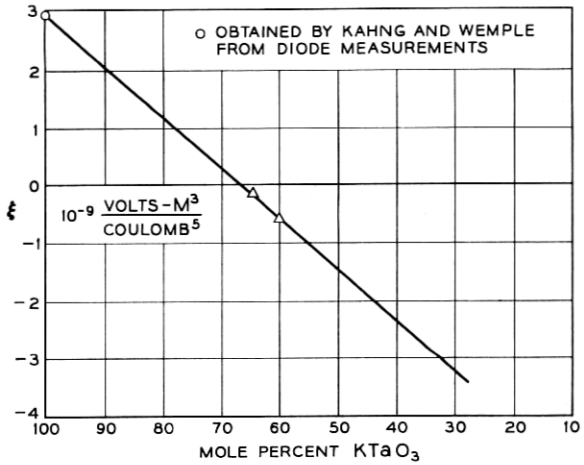

Fig. 6 — Compositional dependence of Devonshire nonlinear parameter ξ.

a typical low field dielectric constant $\kappa \equiv \epsilon/\epsilon_o$ versus temperature curve. Fig. 6 shows a plot of the saturation parameter ξ as a function of composition for KTN. Fig. 7 shows an analogous plot of the phase transition temperature T_o for KTN. Using the information given above we can continue the discussion of biasing and derive conditions for optimizing the bias polarization.

From (12) and the small signal permittivity ϵ_b

$$\epsilon_b = \frac{\epsilon}{1 + 3\epsilon\xi P_b^2 + 5\epsilon\zeta P_b^4 \cdots} \tag{27}$$

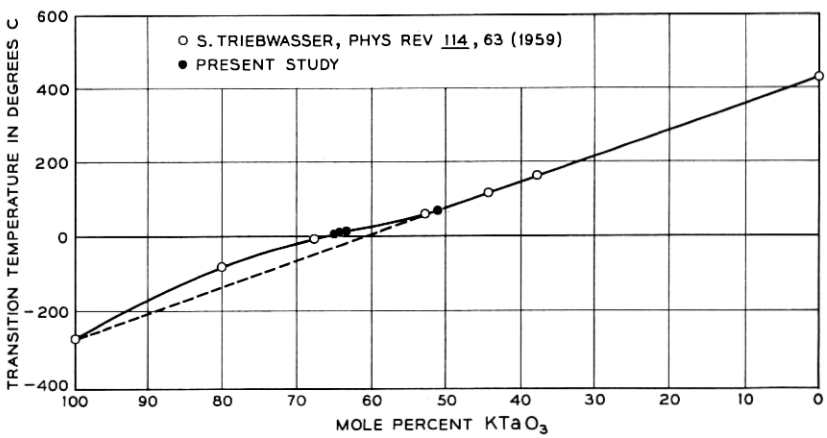

Fig. 7 — Compositional dependence of phase transition temperature in $KTa_xNb_{1-x}O_3$ system.

we see that as the bias polarization is increased, the incremental half-wave voltage has a minimum at,

$$P_b = \left(\sqrt{\frac{2}{15}}\right) P_o \left[1 + \sqrt{1 + \frac{5}{4}\left(\frac{T - T_o}{T_c - T_o}\right)}\right]^{\frac{1}{2}} \tag{28}$$

where P_o is the spontaneous polarization at T_c (see (77)) and $T_c - T_o$ is the difference between the transition temperature and Curie temperature (see (78)). This minimum in incremental half-wave voltage is not necessarily the desired optimum bias point, since it does not correspond to minimum reactive power. The average power dissipated in the sample $\mathcal{P}_d$, assuming it is driven by a square wave of repetitive frequency $\frac{1}{2}\nu_r$, zero-to-peak amplitude $\Delta V_{\pi b}$ and rise time $\sim (1/5\nu_r)$ is

$$\mathcal{P}_d \cong \gamma\left(\frac{\pi C_b (\Delta V_{\pi b})^2 \nu_r}{Q}\right) \tag{29}$$

where γ is approximately 1.2. This expression is derived in Appendix C. Each half cycle of the drive voltage is capable of rotating the plane of polarization by 90°. This is done so that there will be no dc component in the drive signal. The necessity of this restriction is discussed in Section VI.

The reactive power defined in the manner of (15) is given by

$$\mathcal{P}_r = \left(\frac{Q}{2\gamma\pi}\right) \mathcal{P}_d \tag{30}$$

Substitution of this result in (18) gives a capacity-speed product,

$$(R_x R_y)^{\frac{1}{2}} \nu_r \leqq \left(\frac{Q}{2\gamma\pi} \Lambda\right) \mathcal{P}_d \tag{31}$$

where Λ is given by,

$$\Lambda = \frac{3}{20\alpha\beta\lambda\left[1 + \frac{l_m - l}{l}\right]} \tag{32}$$

and

$$\alpha = \frac{1}{2\epsilon_b}\left(\frac{\lambda}{4aP_b}\right)^2. \tag{33}$$

If the upper limit on the dissipated power $\mathcal{P}_d$ is independent of bias polarization then the capacity-speed product has its maximum as a function of bias polarization at

$$P_b = \left(\frac{1}{5\epsilon\zeta}\right)^{\frac{1}{4}}. \tag{34}$$

The reason we have derived an expression for the capacity-speed product in terms of the dissipated power is that the primary limitation on the reactive driver power for a KTN polarization modulator can be directly related to heating caused by power dissipation within the modulator. Since we are dealing with pulse modulation the drive signal contains frequency components substantially higher than the pulse repetition rate ν_r. The Fourier series expansion of a square wave contains all odd harmonics of the fundamental ($\nu_r/2$). In order to obtain an adequate rise time, the system driver plus modulator should encompass as many harmonics as possible (see (92)). If the Fourier series is terminated on the third or fifth harmonic the waveform will be that shown in Fig. 8. This places a restriction on the driver impedance if a flat response is desired. If we assume that the 3-dB power point occurs at a frequency ν_u (which we take to be an odd integer multiple of ν_r) then the generator impedance is given by

$$R_g = \frac{1}{2\pi\nu_u C_b}. \tag{35}$$

Up to this point we have not set any upper limit on the power $\mathcal{P}_d$ dissipated within the modulator crystal. The heating caused by this dissipated power is not negligible. Even in the presence of large heat sinks the finite thermal conductivity of the modulator crystal gives rise to thermal gradients which affect the device performance because we are

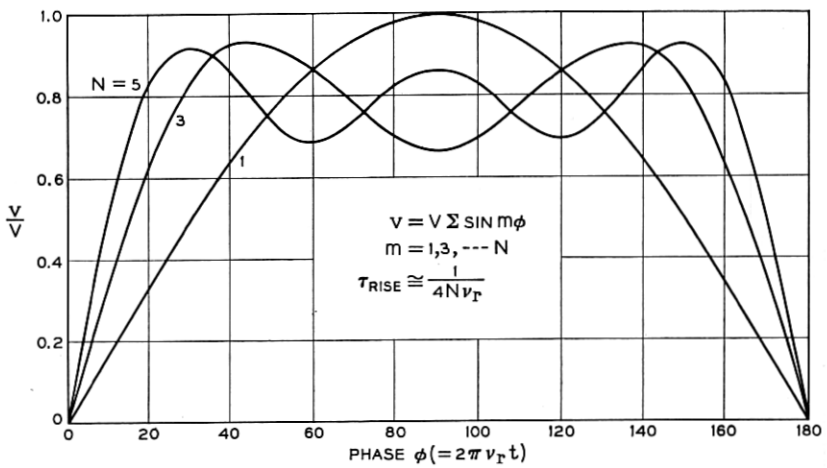

Fig. 8 — Waveshapes of a "square" wave with varying harmonic content.

operating close to the Curie point. These thermal gradients form the basic limitation on the intensity ratio which the modulator can maintain between the two senses of polarization accepted by the Wollaston prisms. Present estimates[9] of the minimum required intensity ratio for the DLD are around 20 dB.* This extinction ratio thus becomes an important design parameter which we shall now introduce into the analysis.

From (9) we can express the phase retardation $\Delta\varphi$ for two light rays traveling along paths of slightly different temperature T and $T + dT$,

$$\Delta\varphi(T + dT) = \Delta\varphi(T) + \frac{\partial\Delta\varphi}{\partial T}\,dT \tag{36}$$

where

$$\frac{\partial\Delta\varphi}{\partial T} = \frac{4\pi a l P_b^{\,2}}{\lambda(T - T_o)}\,.$$

For light polarized at 45° with respect to principal axes of the modulator the transmission functions for the two orthogonal polarization states of the Wollaston deflectors are,

$$\begin{aligned} I_\perp &= I_o \sin^2\left(\frac{\Delta\varphi}{2}\right) \\ I_\parallel &= I_o \cos^2\left(\frac{\Delta\varphi}{2}\right). \end{aligned} \tag{37}$$

If we define Δ as

$$\Delta^{\frac{1}{2}} \equiv \frac{2\pi a l P_b^{\,2} dT}{\lambda(T - T_o)} \tag{38}$$

and take $\Delta\varphi(T) = m\pi$ where m is an even integer then it is readily seen that the extinction ratio has changed from

$$\frac{I_\perp(T)}{I_\parallel(T)} = 0$$

to

$$\frac{I_\perp(T + \Delta T)}{I_\parallel(T + \Delta T)} \cong \Delta \qquad \text{where} \qquad \Delta \ll 1. \tag{39}$$

In order to find Δ as a function of position across the aperture of the modulator, we must solve the heat transfer equation. Assuming that

* A nonlinear optical absorber might reduce this to 10 dB.

the power $\mathcal{P}_d$ given in (29) is dissipated uniformly in the modulator crystal the heat transfer equation can be written,

$$\underline{\nabla} \cdot k \underline{\nabla} T = -\frac{\mathcal{P}_d}{\mathcal{U}} \tag{40}$$

where $\mathcal{U} = bdl$ is the volume of the modulator crystal, k is the thermal conductivity and $T = T(xyz)$ is the temperature function. If cooling is provided primarily at two opposite faces of the modulator (40) reduces to,

$$\frac{\partial^2 T}{\partial x^2} = -\frac{\mathcal{P}_d}{k\mathcal{U}} \tag{41}$$

where x is directed along the cooling surface normal. The solution to (41) is

$$T = T_s + \frac{\mathcal{P}_d}{2k\mathcal{U}}\left(\frac{d^2}{4} - x^2\right) \tag{42}$$

where T_s is the surface temperature and x varies from $-d/2$ to $+d/2$ if cooling is at the electroded faces. Putting this result in (38) and integrating over the aperture bd we find

$$\mathcal{P}_d = \frac{\sqrt{30}\,\lambda k (T_s - T_o)(\bar{\Delta})^{\frac{1}{2}}}{\pi a P_b^2}\left(\frac{b}{d}\right) \tag{43}$$

where $\bar{\Delta}$ is the average extinction ratio over the aperture of the modulator. Substitution of this result in (31) gives the capacity-speed product,

$$(R_x R_y)^{\frac{1}{2}} \nu_r \leqq \left\{\frac{12\sqrt{30}\,aQk(\bar{\Delta})^{\frac{1}{2}}(T_s - T_o)\epsilon_b}{5\pi^2\gamma\beta\lambda^2\left[1 + \left(\frac{l_m - l}{l_m}\right)\right]}\right\}\frac{b}{d}. \tag{44}$$

This expression is independent of bias polarization and to first approximation independent of temperature. The latter statement rests on the condition that at the operating point $(T_s - T_o, P_b)$ dielectric saturation is negligible, (i.e., $\epsilon_b \cong \epsilon = C/(T_s - T_o)$ where C is the Curie constant). For unity aspect ratio (b/d) the capacity speed product is thus primarily determined by material parameters such as thermal conductivity k, electrical quality factor Q, Curie constant C, etc. The only adjustable parameters are the extinction ratio $(\bar{\Delta})$, wavelength λ, and resolution limit β. In many instances these will be determined by the choice of memory plane in a particular application. The short wavelength limit of the modulator above is determined by the width of the forbidden energy gap (in KTN 3.45 eV), which restricts use of KTN to wave-

lengths longer than 4000 Å. The advantage of using a rectangular aperture is also evident from (44). For a specific operating speed the total capacity increases linearly with the aspect ratio. Even a modest 3:1 ratio give a factor of 6 improvement in capacity. The optical image of the source is of course distended by roughly the same ratio (b/d) but for many applications this might not be a limitation.

An expression for the generator impedance R_g can be derived if we let $\nu_u = \frac{5}{2}\nu_r$ in (35) and substitute (12), (29), and (43),

$$R_g = \frac{\pi\gamma\lambda}{80\sqrt{30}\, aQk(\bar{\Delta})^{\frac{1}{2}}\epsilon_b^2(T_s - T_o)}\left(\frac{d}{b}\right)\left(\frac{d}{l}\right)^2. \tag{45}$$

IV. APPLICATION OF THE DESIGN EQUATIONS TO A 10^6 ADDRESSES/SEC DLD SYSTEM UTILIZING KTN MODULATORS

In order to obtain a better idea of the implications of the various relations derived in the preceding sections it is necessary at this point to substitute some of the physical constants. Taking the values of the constants listed in Table I, we can evaluate the capacity-speed product from (44),

$$(R_xR_y)^{\frac{1}{2}}\nu_r \leqq \frac{7{,}950(\bar{\Delta})^{\frac{1}{2}}}{1 + \left(\frac{l_m - l}{l_m}\right)}\left(\frac{b}{d}\right) \text{ addresses MHz.} \tag{46}$$

The choice of $\beta = 4$ is based on an extrapolated improvement of 2 in the value of 8 obtained by Tabor[9] in a DLD using passive modulators.

Taking an extinction ratio of 20 dB ($\bar{\Delta} = 0.01$) and a speed of 10^{-6} sec/address we obtain from (46) the maximum capacity,

$$(R_xR_y)^{\frac{1}{2}} = \frac{795}{1 + \left(\frac{l_m - l}{l_m}\right)}\left(\frac{b}{d}\right) \text{ addresses.} \tag{47}$$

It is therefore, advantageous to make $(l_m - l)/l_m$ as small as possible.

The Wollaston prisms, plus support sections, plus clearance (i.e.,

TABLE I

Thermal conductivity k	50 mW/cm °C
Electrical quality factor Q	1000 (at 1 MHz)
Electro-optic parameter a	1.13 m^4/coulomb^2 (at 5000 A)
Curie constant	1.4×10^5 °K^{-1}
Light wavelength	5000 Å
Resolution factor β	4

$l_m - l$) can be conservatively set at a lower limit of 2 mm. Let us first consider the case of a square aperture (i.e., $b = d$). For this case, (6) becomes

$$A \geqq \frac{4}{3} l_m 10^{-3} R(\text{cm}^2) \tag{48}$$

where

$$R_x = R_y = R.$$

Taking $l_m = 1$ cm ($l = 0.8$ cm) we arrive at the modulator and DLD characteristics shown in Table II. Increasing l_m beyond 1 cm (e.g., to 2 cm) would only increase the capacity by 20 percent. The operation of a 10^6 bit/sec DLD system with a square aperture using KTN modulators is thus limited to a capacity of about 0.5×10^6 addresses. However, several factors which have been neglected serve to further limit this capacity. These factors are discussed in the next two sections, as is the rectangular aperture which enables the capacity to be increased to 10^6 addresses.

V. Effects of Compositional Inhomogeneities and Ambient Temperature Fluctuations on KTN Modulator Performance

Compositional inhomogeneities occur during the growth of KTN crystals[10] which give rise to fluctuations in the Curie temperature throughout the crystal. The exact nature of the inhomogeneities and their elimination is beyond the scope of this paper. The relevant point in this discussion is that Curie temperature variations do exist and should be included in the modulator analysis. Examination of (38) shows that we can extend the interpretation of dT as

$$dT = d(T - T_o) = dT(x,y) + dT_s - dT_o(x,y). \tag{49}$$

Table II — Performance Characteristics of DLD using KTN Modulator

Modulator dimensions	$b = d = 0.92$ cm $l = 0.8$ cm
DLD capacity	0.4×10^6 addresses
DLD speed	10^{-6} seconds/address
Dissipated power	9.7 mW
Reactive power	1.3 W
Generator impedance	65 Ω
Bias polarization	2 μ coulombs/cm^2
Bias voltage	1500 V
Driver voltage	51 V
Number of half-waves bias	15
Capacitance of modulator	1000 pF

In the previous treatment of Sections III and IV we neglected dT_s and dT_o. From (42) we can calculate $dT(x = 0)$ for a dissipated power of 10 mW, a volume of 0.65 cm^3 and $d = 0.92$ cm corresponding to the modulator discussed in Section IV, and find

$$dT(x = 0) = 0.03°\text{C}. \tag{50}$$

The previous analysis is thus valid for dT_s and dT_o much less than 0.03°C. This corresponds to temperature regulation in the thousandths of a degree region which is within capabilities of present technology but requires some sophistication and cost.

Curie temperature variations occurring during growth are presently[11] in the range 1°C to 10°C for samples several mm's on a side. To hold variations of 0.01°C requires a control of the solid-solution to within roughly 20 ppm of the 65/35 mixture. Let us for the sake of discussion see what effect a constant variation $\delta \equiv \Delta T_s - \Delta T_o$ of 0.01°C would have on the derivation of (43). The result of this calculation is the following equation,

$$\mathcal{P}_d = \frac{2k\mathcal{U}}{d^2}\left[-\frac{5}{2}\delta + \frac{1}{2}\left\{-95\delta^2 + 120\bar{\Delta}\left(\frac{\lambda(T_s - T_o)}{2\pi a P_b{}^2 l}\right)^2\right\}^{\frac{1}{2}}\right]. \tag{51}$$

For $\delta \to 0$, $\mathcal{P}_d$ of course reduces to the expression given in (43). For $\delta \neq 0$ the negative sign in the radical, combined with the requirement that $\mathcal{P}_d$ be a real positive quantity, indicates that there is a lower limit to the quantity $[(\lambda(T_s - T_o)/2\pi a P_b{}^2 l]$. The previous analysis did not place any limit on $T_s - T_o$ and P_b ; and l_m could be made larger if A was increased. The additional restriction coming from (51) leads to a modified capacity-speed product,

$$(R_x R_y)^{\frac{1}{4}} \nu_r \leqq \frac{24a^2 Qk\epsilon_b (P_b{}^2 l)\left[-\frac{5}{2}\delta + \frac{1}{2}\left\{-95\delta^2 + 120\left(\frac{\lambda(T_s - T_o)}{2\pi a}\right)^2\left(\frac{1}{P_b{}^2 l}\right)^2\bar{\Delta}\right\}^{\frac{1}{2}}\right]\left(\frac{b}{d}\right)}{5\pi\gamma\beta\lambda^3\left[1 + \left(\frac{l_m - l}{l}\right)\right]}. \tag{52}$$

Remembering that $l_m - l/l_m < 1$ it can be shown that the capacity-speed product has a maximum, as a function of $P_b{}^2 l$ at

$$P_b{}^2 l = \sqrt{\frac{5}{19}}\,\frac{(\bar{\Delta})^{\frac{1}{2}}\lambda(T_s - T_o)}{2\pi a\delta} \tag{53}$$

and goes to zero at,

$$P_b^2 l = \frac{(\bar{\Delta})^{\frac{1}{2}} \lambda (T_s - T_o)}{2\pi a \delta} . \tag{54}$$

Putting the values $\lambda = 5000$ Å, $(T_s - T_o) = 10°\text{C}$, $a = 1.13$ m^4/coulomb^2, and $\delta = 0.01°\text{C}$ into (53) and (54) we find $R\nu_r$ has a maximum at

$$P_b^2 l = 3.6 \frac{(\mu \text{ coulomb})^2}{\text{cm}^3} \tag{55}$$

and zero at

$$P_b^2 l = 7 \frac{(\mu \text{ coulomb})^2}{\text{cm}^3} . \tag{56}$$

In the earlier calculation of Section III where $\delta = 0$ we arrived at the values $P_b = 2$ μ coulombs/cm^2 and $l = 8$ mm giving $P_b^2 l = 3.2$ which is only slightly smaller than the optimum above. Using the parameters in Table I and taking $T_s - T_o = 10°\text{C}$ we can write (52) as

$$R\nu_r \leqq \frac{2010 P_b^2 l \left[-\frac{5}{2}\delta + \frac{1}{2}\left\{ -95\delta^2 + \frac{61\Delta}{(P_b^2 l)^2} \right\}^{\frac{1}{2}} \right]}{\left[1 + \left(\frac{l_m - l}{l_m} \right) \right]} \cdot \frac{b}{d} \text{ address-MHz.} \tag{57}$$

Putting $P_b^2 l = 3.6$ μ coulomb 2/cm^3, $\bar{\Delta} = 0.01$ and $\delta = 0.01°\text{C}$, $\nu_r = 1$ MHz, and $l = 8$ mm into (57) we find the maximum capacity is 0.18×10^6 addresses. This is 35 percent lower linear capacity (418) than the maximum linear capacity (635) obtained when δ was assumed to be negligible. It can in fact be shown that if $P_b^2 l$ is chosen to satisfy (53) then the capacity-speed products in (44) and (52) are related by a constant multiplier,

$$(R\nu_r)_{\delta \neq 0} = (R\nu_r)_{\delta=0} \left[\left(1 - \frac{95}{456} \right)^{\frac{1}{2}} - \frac{5}{\sqrt{456}} \right] = 0.656 (R\nu_r)_{\delta=0} . \tag{58}$$

Thus, the primary effect of introducing compositional nonuniformities and ambient temperature fluctuations has been to decrease the capacity-speed product by 35 percent, and also to prescribe an optimum value for $P_b^2 l$ given by (53). It is interesting to note that for $l > 2$ mm the value of P_b obtained in this fashion is substantially less than the value required to minimize the power or drive voltage (see (28) and (34)). Since $P_b^2 l$ from (53) is proportional to $1/\delta$ an increase in δ beyond 0.01°C would reduce $P_b^2 l$ to less than 3.6 μ coulombs^2/cm^3. A substantial

increase in δ beyond 0.01°C is not desirable, however, since l must be greater than 2 mm to prevent the denominator in the capacity-speed product from becoming large, and secondly P_b cannot be reduced much below 2.0 μ coulombs/cm^2 as the drive voltages become excessive. Thus, it is clear that close temperature regulation to several hundredths of a degree, and precise control of chemical composition to tens of ppm are both essential. In the next section, an ac biasing scheme is discussed which relaxes these requirements.

Table III lists the new operating characteristics for a square aperture system which result from the modified design equations derived in this section.

VI. SPACE CHARGE EFFECTS AND AC BIASING

In this section, we shall consider the adverse effects of finite electrical conductivity in the presence of a dc bias, and discuss the ac biasing scheme proposed by Warter[12] for overcoming these effects. We shall also consider the advantages of a rectangular aperture and the problems associated with finding other materials than KTN for use as the active electro-optic medium.

The static electrical conductivity of KTN in the vicinity of 300°K falls in the range 10^{-11} to 10^{-12} mhos/cm. This conduction has been demonstrated to be extrinsic and due to holes having a very low trap controlled mobility of 10^{-6} cm^2/V sec. The filled acceptor level density is less than 10^{13}/cm^3 and is peaked around 0.6 to 0.8 eV above the valence band.

This small but finite conductivity gives rise to several types[13] of nonuniform electric polarization distribution within the sample when a dc electric field is applied. The type of nonuniformity and the associated time constant depend on the nature of the electrical contact (e.g., ohmic

TABLE III — PERFORMANCE CHARACTERISTICS OF DLD USING KTN MODULATOR IF δ = 0.01°C

Modulator dimensions	$b = d = 0.75$ cm $l = 0.8$ cm
DLD capacity	0.18×10^6 addresses
DLD capacity-speed product	0.42×10^9 sec^{-1}
Dissipated power	6.4 mW
Reactive power	0.86 W
Generator impedance	43 Ω
Bias polarization	2 μ coulombs/cm^2
DC bias voltage	1200 V
Driver voltage	42 V
Number of half-waves bias	15
Capacitance of modulator	1000 pF

or blocking). In the case of blocking contacts[14] two phenomena occur with different time constants. The first effect is the build-up of a space charge in the vicinity of nonuniform conductivity and/or nonuniform dielectric constant. It can be shown from Maxwells equations that the time constant for this build-up is approximately given by the dielectric relaxation time,

$$\tau_r = \rho\kappa\epsilon_o \tag{59}$$

where ρ is the average resistivity and κ the average dielectric constant. For a dielectric constant of 10^4 and a resistivity of 10^{12} Ω-cm, τ_r is of the order of 10^3 seconds. The second effect is the formation of a depletion layer[14] in the vicinity of the blocking (positive for p-type conduction) electrode. The time constant for depletion layer formation is given by,

$$\tau_{sh} = \frac{d(\infty)L}{2\mu_{eff}V} \tag{60}$$

where $d(\infty)$ is the final depletion layer width

$$d(\infty) = \sqrt{\frac{2\epsilon V}{N_T e}}$$

and L is the electrode separation, N_T is the density of filled trapping levels, and μ_{eff} is the trap-controlled or "effective" mobility. For KTN having a resistivity of 10^{12} ohm-cm this depletion layer buildup time is between 10^3 and 10^4 seconds.

In the case of ohmic contacts[14,15] space charge buildup can occur due to nonuniformities in the conductivity, as in the case of blocking contacts, or a space charge may also occur which is associated with operation in range of space charge limited current flow. It can be shown that the transition from ohmic current flow to space charge limited current flow occurs when

$$V > \frac{8}{9}\left(\frac{N_T e L^2}{\epsilon}\right). \tag{61}$$

The large dielectric constant of KTN causes this transition to occur at much lower current levels than in other materials.

The nonuniformities in polarization caused by each of these effects exceeds that which the system can tolerate by several orders of magnitude. While the possibility of a direct solution to the dc bias problem cannot be ruled out, two alternatives exist which eliminate the need for a dc bias. The first of these involves operation of the modulator in the ferroelectric region[16,17] with the spontaneous polarization acting as the

bias polarization. The previous analysis of Sections II to V is applicable to this case except that the dielectric constant no longer obeys a Curie-Weiss law but varies in the fashion described by (82) in Appendix C. The temperature dependence of the spontaneous polarization is also different, which changes the derivation of (43).

A comparison of (80) and (81) shows that the dielectric constant drops discontinuously to 1/4 of its peak value at the phase transition. For KTN with a transition temperature of 10°C this means a drop from 36,000 to 9,000. Thereafter, it drops to below 2,000 within a temperature range of less than 10°C. If one modifies the analysis of the preceding sections to take these facts into account, one finds that ferroelectric biasing further reduces the maximum capacity by a factor of at least 4. The further assumption is made here that large samples will remain single domain when operated within 5 to 10°C of the Curie point.

A second biasing scheme which does not appear to have this liability has been proposed by P. J. Warter, Jr.[12] The basic idea in Warter's scheme is to use two modulator crystals in series (1 and 2). An ac bias source provides separate current drives in quadrature to the two sections, as indicated in Fig. 9 for one of the two modulators,

$$\begin{aligned} i_1 &= i_o \sin \omega_o t \\ i_2 &= i_o \cos \omega_o t. \end{aligned} \tag{62}$$

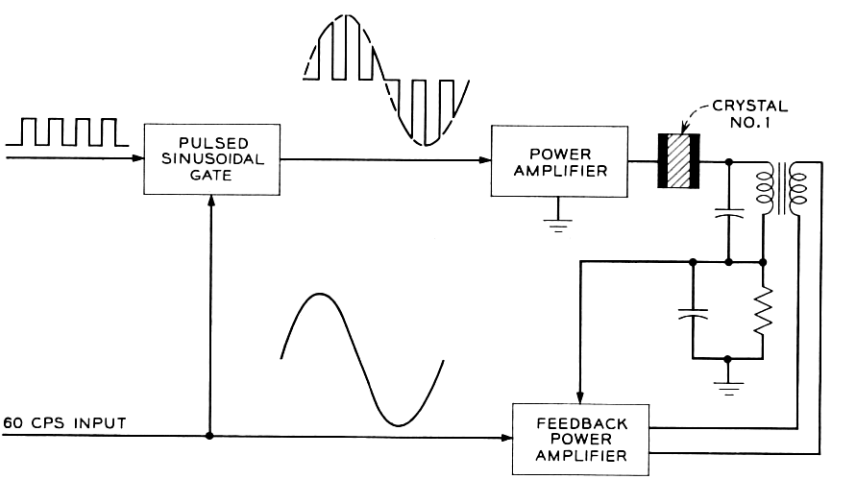

Fig. 9 — Block diagram of driver circuit for modulator 1 in Warter's ac bias scheme.

The charge on the electrodes of the two samples produces an electric polarization in the sections which varies as

$$\begin{aligned} P_1 &= P_o \cos \omega_o t \\ P_2 &= P_o \sin \omega_o t \end{aligned} \tag{63}$$

where $P_o = i_o/\omega_o A$, A being the electrode area. The phase retardation through the two sections is the sum of retardations in each section and hence,

$$\Delta\varphi = \frac{2\pi}{\lambda} a(P_1^2 + P_2^2)\ell = \frac{2\pi a}{\lambda} P_o^2 \ell \tag{64}$$

with P_o being the bias polarization. Since the bias signal on each section contains no dc component the previously discussed conduction phenomenon does not occur if the contacts are electrically blocking and the period $\tau_o = 2\pi/\omega_o$ is short compared to the dielectric relaxation period τ_r.

In addition the use of a current drive rather than a voltage drive insures a constant polarization along a path normal to the electrodes (x direction) even if the temperature changes slightly. This also holds for nonuniform temperature variations along the same path within the sample. The electric fields adjust internally for regions of varying dielectric constant such as to maintain uniform polarization along the x direction. This relaxes the stringent requirements on ambient temperature control and chemical homogeneity. A detailed analysis of the limitations of the ac bias is needed before any reliable statements can be made as whether it will allow a significant increase in the capacity speed products calculated in the previous sections. Such an analysis depends critically on distortions in the drive signal from a pure sinusoidal behavior which are not known at present. It should be noted that each modulator in this scheme must be the same length l as a single modulator in the previous analysis, giving a reduction of 4 (see (20)) in the capacity R^2 if the cross-sectional area A is held constant.

Another adverse optical effect which has been observed in dc biased KTN polarization switches occurs when the diameter of the optical beam (of several mW power) is reduced to around 0.2 mm. Under these conditions a severe distortion of the optical transmission function from its expected form (see (37) and Fig. 3) was observed as shown in Fig. 10. If the light was switched on rapidly (in <0.1 sec.) the initial transmission function was that shown in Fig. 3, but went over into that shown in Fig. 10 after several seconds of illumination. If the light beam was moved rapidly to a different region the same sequence was observed. A return

to the original spot gave the pattern in Fig. 10 without any buildup time, indicating that the cause of the refractive index distortion was still present, and had not decayed after many seconds. Insertion of 30 dB of optical attenuation in the input beam was found to completely eliminate the occurrence of distortion. Further measurements[18] suggest that the distortion is being produced by an internal bias field acting in opposition to the applied field but nonuniformly distributed in the immediate vicinity of the affected area. Since no distortion was observed in the absence of a dc bias field one is tempted to postulate that the intense light beam is generating some sort of charged centers or charge carriers which drift under the influence of the external field and are then trapped near the edge of beam. Chen[18] and Boyd[19] have made further optical measurements of the distortion of the refractive index ellipsoid of KTN in the vicinity of beam which indicate that the effect being described here may be related to "optical damage" effects observed recently in $LiNbO_3$ and $LiTaO_3$.

Since no satisfactory explanation of either effect is available at the present time we shall conclude this discussion by noting that this problem is not one of concern for the DLD polarization switch since optical levels will probably be somewhat less than 0.1 W/cm^2, and for KTN the ac bias scheme of Waters would circumvent the problem even at high light levels.

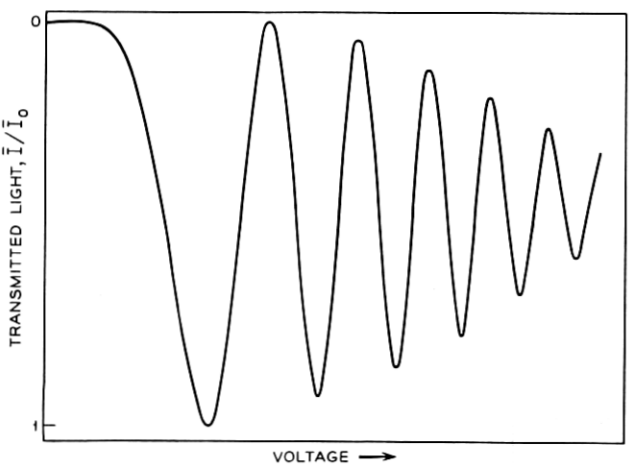

Fig. 10 — Light transmitted by optically "damaged" region of KTN polarization switch.

VII. RECTANGULAR APERTURE AND COMPARISON OF LINEAR ELECTRO-OPTIC MATERIALS WITH KTN

7.1 *Rectangular Aperture*

It was shown in Section II that the capacity speed product depended primarily on the amount of power one can use to drive the modulator. In Section III we showed that this power for KTN is limited by the extinction requirements of the DLD. Holding the extinction constant it was shown that one could increase this power hence the capacity-speed product by using a rectangular aperture (i.e., $b/d > 1$). This conclusion was unchanged when Curie temperature variations and ambient temperature fluctuations were included (see (52)). Let us consider the improvement which a modest aspect ratio of 3:1 ($= b/d$) can make in the capacity-speed product of the KTN modulator described in Section V. Table IV lists the operating characteristics of a KTN nodulator with $b/d = 3$. The capacity can therefore, be brought up to the megabit region with only a modest 3/1 aspect ratio, while maintaining reasonable driver requirements, well within the capabilities of transistor circuitry.

7.2 *Comparison of Linear Electro-optic Materials with KTN*

In Section II it was shown that the capacity-speed product for different electro-optic modulator materials (e.g., A and B) being driven with identical reactive powers differed only in the factor (see (20)).

TABLE IV — PERFORMANCE CHARACTERISTICS OF DLD USING KTN AND RECTANGULAR APERTURE

Modulator dimensions	$b = 2.24$ cm $d = 0.75$ cm $l = 0.8$ cm
DLD capacity	1.0×10^6 addresses
R_x	422
R_y	3700
DLD capacity-speed product	1.0×10^9 sec^{-1}
Dissipated power	19 mW
Reactive power	2.6 W
Generator impedance	15 Ω
Bias polarization	2 μ coulombs/cm^2
dc bias voltage	1200 V
Driver voltage	42 V
Number of half-wave bias	15
Capacitance of modulator	3000 pF
Dielectric constant	14,000
Reduced biased half-wave voltage	45 V

$$\frac{[(R_xR_y)^{\frac{1}{2}}\nu_r]_A}{[(R_xR_y)^{\frac{1}{2}}\nu_r]_B} = \frac{\alpha_B\left(1 + \frac{l_m - l}{l}\right)_B}{\alpha_A\left(1 + \frac{l_m - l}{l}\right)_A}. \tag{65}$$

Since we assumed that $l_m - l/l_m$ is small, the comparison of different modulator materials reduces to a comparison of their α's. To facilitate this comparison we put (17) for biased quadratic-electro-optic materials in the form,

$$\alpha = \frac{\epsilon_b}{2}(\Delta v_{\pi b})^2 \tag{66}$$

where $\Delta v_{\pi b} = \Delta V_{\pi b}(l/d)$ is the reduced half-wave voltage for the biased material,

$$\Delta v_{\pi b} = \frac{\lambda}{4aP_b\epsilon_b}. \tag{67}$$

For the KTN modulator described in Table IV, α/ϵ_o has the value 1.4×10^7 $(\text{V})^2$. For a linear electro-optic material with a dielectric constant of $10\epsilon_o$, a reduced half-wave voltage of 1670 volts would be required to give the same value of α as the biased KTN.

In the past the lowest reported[5] reduced half-wave voltage for a linear transverse effect was 6200 volts for cuprous chloride. Recently both lithium niobate[20] and zinc telluride[6] have been shown to have reduced half-wave voltages of less than 5 kV. Lithium niobate has the disadvantages of a somewhat higher dielectric constant and an appreciable natural birefringence which would tend to limit the angular aperture. Zinc telluride has a relatively small optical band gap ($\sim$2 eV) and would be restricted to use at wavelengths >6000 Å. Nevertheless, it is significant that materials with a sufficiently large linear transverse electro-optic effect and low dielectric constant do exist. Table V lists the capacity-speed product and several other operating characteristics of a DLD designed using $LiNbO_3$ and ZnTe. One of the principal advantages is relative insensitivity of these materials to temperature changes. This means that larger reactive powers may be used if one can meet the drive voltage requirements. The rectangular aperture again offers an advantage by allowing a reduction in this drive voltage while maintaining a high capacity. This fact has been used in deriving the numbers in Table V.

TABLE V — COMPARISON OF KTN WITH LINEAR ELECTRO-OPTIC MATERIALS

	$LiNbO_3$*	ZnTe†	KTN‡
Modulator dimensions b	2.64 cm	2.64 cm	2.24 cm
d	0.5 cm	0.5 cm	0.75 cm
l	1 cm	1 cm	0.8 cm
Reduced half-wave voltage v_π	400 V	2500 V	45 V
Dielectric constant	40	10	14,000
Capacity-speed product	1.9×10^8 sec^{-1}	1.9×10^9 sec^{-1}	1.0×10^9 sec^{-1}
Capacity	3.6×10^4 add.	3.6×10^6 add.	1.0×10^6 add.
Speed	10^{-6} sec/add.	10^{-6} sec/add.	10^{-6} sec/add.
Driver voltage	2000 V	1250 V	42 V
Reactive power 10 W	10 W	10 W	2.6 W
α/ϵ_o	3.2×10^8 (V)^2	3.1×10^7 (V)^2	1.4×10^7 (V)^2
DC bias voltage	0 V	0 V	1200 V
Capacitance	19 pF	4.6 pF	3000 pF
Heating ΔT	0.04°C	0.4°C	0.02°C

* $\lambda = 5000$ Å, $Q = 1000$.
† $\lambda = 6000$ Å, $Q \sim 100$.
‡ $\lambda = 5000$ Å, $Q = 1000$, dc bias.

VIII. SOME EXPERIMENTAL RESULTS

Because of the large composition fluctuations in presently available KTN mentioned in Section V the experiments described in this section were carried out using much smaller samples than those needed for a 10^6 address DLD system. Samples were generally several mm on a side. Pulse experiments were performed using the circuit shown in Fig. 11. At slow sweep speeds, around 1 msec/cm, the expected modulation waveforms (see Fig. 12) were observed with 100 percent modulation occurring when the pulse height equaled the dc incremental half-wave voltage. For faster sweep speeds in the 1 μsec/cm range, a strong ringing of the

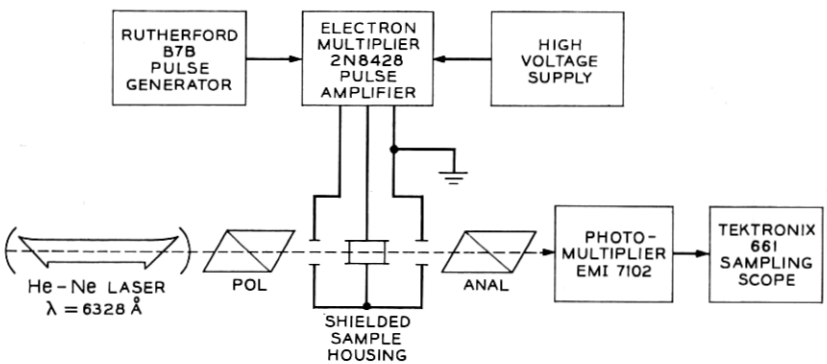

Fig. 11 — Experimental apparatus for unbiased pulse measurements.

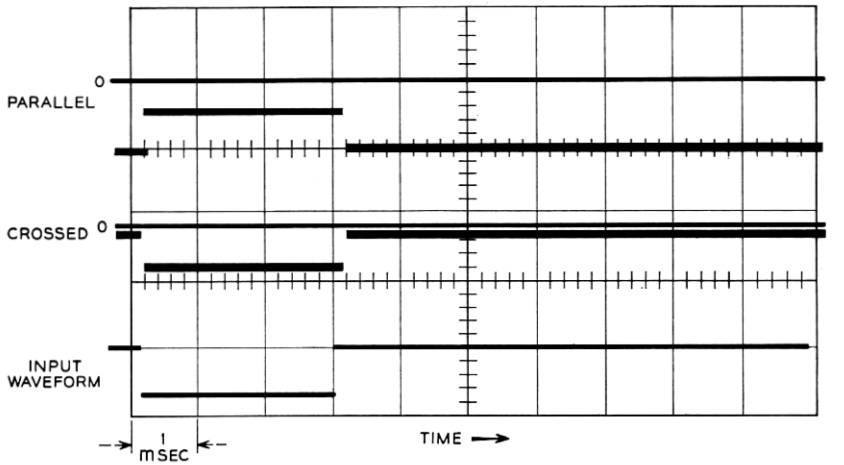

Fig. 12 — Very low frequency light modulation response.

light intensity following the leading and trailing edges of the pulse was observed. The damping of these oscillations was small. Analysis with a Rohde Schwartz receiver showed that a number of frequencies were being superposed and that these corresponded approximately to the low-order mechanical vibration modes[21] of the sample. Typical responses are shown in Figs. 13 and 14. In Figs. 14(a) and 14(b) the pulse width

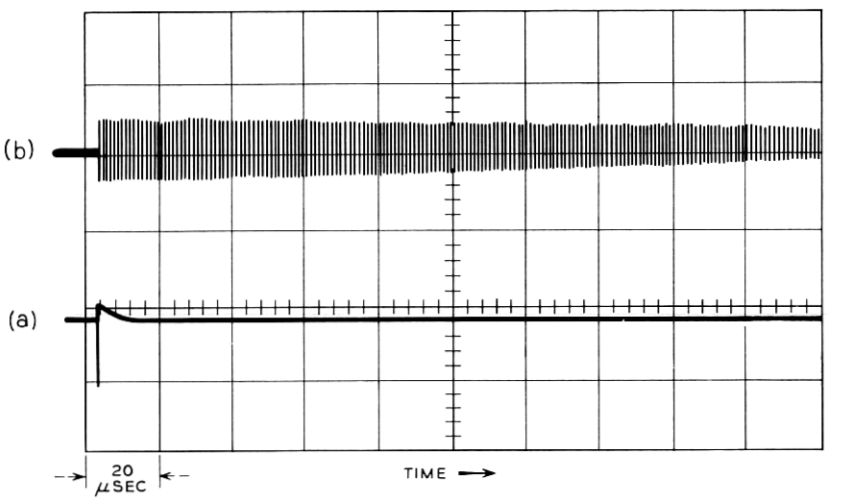

Fig. 13 — Ringing in light modulation at intermediate pulse widths (several μsec).

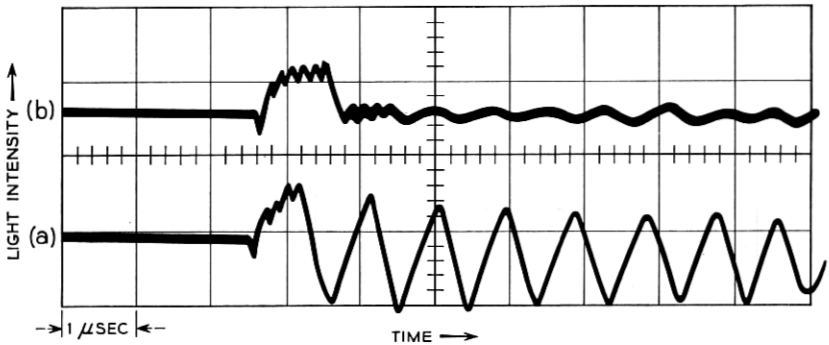

Fig. 14 — Interference effects induced by varying the pulse widths.

has been adjusted to give, respectively, constructive and destructive interference. The dominant frequency excited is that corresponding to the fundamental longitudinal thickness mode. A further study with sine wave excitation revealed that in the unbiased case, resonant excitation of this mode occurred at $\nu_{\text{drive}} = \frac{1}{2}\nu_{\text{fundamental}}$ corresponding to electrostrictive excitation. In the presence of a bias field, excitation occurred at $\nu_{\text{drive}} = \nu_{\text{fundamental}}$ corresponding to piezoelectric excitation. An effective (or induced) piezoelectric coefficient d_{33} can be calculated for a bias polarization P_b from the relation

$$d_{33} = \left[2Q_{11} - Q_{12}\left(\frac{2s_{12}^{D}}{s_{11}^{D} + s_{12}^{D}}\right)\right] P_b \epsilon_b$$

where s_{ij} are the elastic compliances measured at constant electric displacement, and Q_{ij} are the electrostrictive constants.

It was found possible to partially damp these acoustic resonances by two methods. In the first method, the sample and electrodes were imbedded in Armstrong epoxy but the faces through which the light passed were left unobstructed. In the second technique cold-worked aluminum was bonded to the electrodes. An example of the partially damped response is shown in Fig. 15. An interesting feature clearly illustrated in this figure is the initial primary or high-frequency electro-optic response followed by the secondary or elasto-optically induced response having a rise time characteristic of the acoustic travel time across the sample. The clamping effect on the induced birefringence can be estimated from the pulse data to be 25 ± 10 percent for the unbiased crystal. This is in agreement with calculations based on thermodynamic arguments.[3] Both clamping effects and acoustic damping have been neglected in the

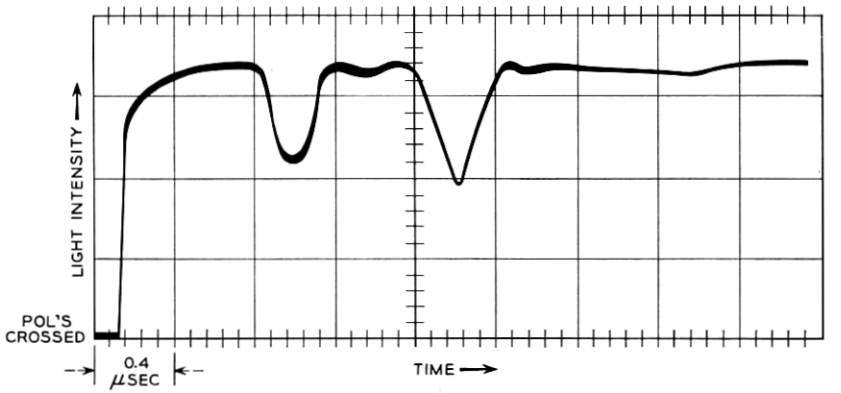

Fig. 15 — Partial damping of acoustic ringing by imbedding in epoxy.

previous sections. Clamping will raise the voltage and power requirements and thus further restrict the capacity. Acoustic damping may be difficult to achieve in practice on large samples without introducing strain. It may also have an adverse effect on the electrical Q in the frequency region near the acoustic resonances. Electrical Q's of several thousand (and up to 10,000) have been measured for KTN up to frequencies of several MHz on undamped samples.

Pulse response has also been measured in the nano-second range at 100 per cent modulation levels. A typical sampling scope trace is shown in Fig. 16. The modulation voltage pulse was delivered by a Huggins nanosecond pulse generator. The signal was detected in an EMI 7102 photomultiplier terminated in the 50 ohm input impedance of a Tektronix Model 660 Sampling scope. The sample was unbiased with a half-wave voltage about 25 percent larger than the measured dc value.*

IX. CONCLUSIONS

An analysis of the modulator requirements for a high capacity-high speed digital light deflection system has been carried out. A principal result of this analysis is the derivation of a simple capacity-speed product

$$(R_x R_y)^{\frac{1}{2}} \nu_r \leqq \Lambda P_r$$

where Λ is essentially a constant characteristic of a given modulator material, and P_r is the reactive power with which the modulator is

* The triangular shape observed was identical to the input voltage waveform. The triangularity was due to current limitations, the driver being unable to provide the current necessary for a sharp leading and trailing edge.

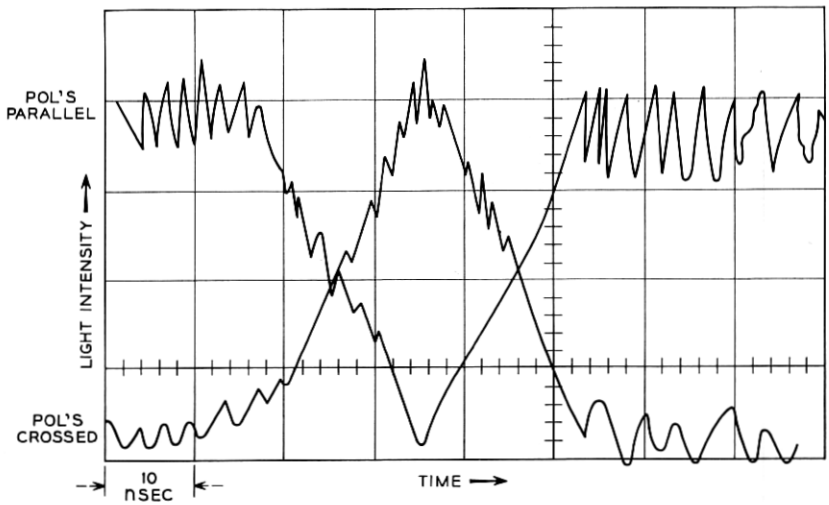

Fig. 16 — Clamped electro-optic pulse modulation.

driven. By examining the limitations on this reactive power one can then compare the performance of different modulator materials in terms of their respective capacity-speed products. For KTN the capacity-speed product is limited to 1.25×10^9 sec^{-1} by the effects of internal heating, assuming ambient temperature fluctuations are held to less than 0.01°C, and compositional nonuniformities affecting the Curie temperature are less than 20 ppm. Presently available KTN has compositional nonuniformities 100 to 1000 times greater than this. In addition further complications arise from the dc bias in the form of space-charge effects. An ac bias scheme proposed by Warter can be used to eliminate space-charge effects. It is thus clear from the foregoing analysis that the material requirements imposed on the KTN to achieve a capacity-speed product of 10^9 sec^{-1} (i.e., 10^6 addresses at a 1 MHz rate) are severe. It is therefore, important to look for other materials where the requirements might not be as severe.

The capacity-speed product is very helpful in such a search since it shows that a linear electro-optic material such as ZnTe with a dielectric constant of 10 and a reduced half-wave voltage of less than 3 kV, has a capacity-speed product of 2×10^9 sec^{-1} for 10 watts reactive power. The capacity-speed products of all other known linear electro-optic materials are less than 2×10^8 sec^{-1}. On the basis of this study there are at present* only two electro-optic materials which are potentially capable

* Note added in proof: Recent work of Denton, Chen, and Ballman (to be published) on $LiTaO_3$, $x_{11} = 43$, $v_\pi = 2700$ V indicates that this material also has a high-capacity speed product.

of operating in a high-capacity high-speed DLD, namely: KTN and ZnTe.

X. ACKNOWLEDGMENTS

The author would like to express his sincere thanks to K. D. Bowers and S. H. Wemple for many invaluable discussions as well as a critical reading of the manuscript. Appreciation is also extended to L. G. Van Uitert and W. B. Bonner for supplying the KTN samples, to M. C. Huffstuttler Jr., R. Curran and R. L. Barns for their results on compositional nonuniformities in KTN, to W. J. Tabor for his experimental results on the DLD system, and to R. T. Denton and E. H. Turner for helpful discussions on ZnTe.

APPENDIX A

Walk-Off Derivation

We assume modules of constant length l_m consisting of a polarization switch of length l and a Wollaston prism of length $l_m - l$. The length of the Wollaston is assumed to be small compared to l_m so that $l_m \sim l$. Starting from the input the modules are arranged in order of increasing angular deflection, in x,y pairs; e.g., $\pm\theta_{x1'}$, $\pm\theta_{y1'}$, $\pm\theta_{x2'}$, $\pm\theta_{y2'}$, $\cdots$, etc. Consider the transverse displacement of the beam at the output of the $x1',y1'$ modules. In the x' direction the beam is displaced by a distance $l_m\theta_{x1'}$ and in the y' direction it is undisplaced in the present approximation. The beam at this same point projected onto the x'-z plane (z is the principal axis of the DLD) makes an angle $\theta_{x1'}$ with respect to the z axis, and projected onto the y'-z plane an angle $\theta_{y1'}$ with respect to the z axis. At the output of $x2',y2'$ modules the corresponding displacements and angles are respectively $5l_m\theta_{x1'}\{= l_m\theta_{x1'} + (2l_m)\theta_{x1'} + l_m\theta_{x2'}\}$, $2l_m\theta_{y1'}\{= 0 + (2l_m)\theta_{y1}\}$, $3\theta_{x1}(= \theta_{x1'} + \theta_{x2'})$, and $3\theta_{y1'}(= \theta_{y1'} + \theta_{y2'})$. Table VI lists these displacements and the succeeding ones. In terms of the diffraction $\theta_D = \lambda/d_j$,

$$\Delta x' \cong \frac{3}{2}\beta_x l_m \frac{\lambda}{d_{x'}} 2^n \tag{68}$$

$$\Delta y' \cong \beta_y l_m \frac{\lambda}{d_{y'}} 2^n . \tag{69}$$

APPENDIX B

Derivation of Capacity-Speed Product for Rectangular Aperture

Remembering that the modulator axes x,y (parallel respectively to the d and b dimensions of the modulator) are rotated 45° with respect to

TABLE VI — LINEAR DISPLACEMENT OF BEAM AT OUTPUT OF iTH PAIR OF MODULES

	Δx	Δy
$i = 1$	$l_m\theta_{x1'}$	0
2	$2l_m\theta_{x1'}(1 + \frac{3}{2})$	$2l_m\theta_{y1'}$
3	$2l_m\theta_{x1'}(1 + 3 + \frac{7}{2})$	$2l_m\theta_{y1'}(1 + 3)$
4	$2l_m\theta_{x1'}(1 + 3 + 7 + \frac{15}{2})$	$2l_m\theta_{y1'}(1 + 3 + 7)$
⋮	⋮	⋮
n	$2l_m\theta_{x1'}\left[\sum_{j=1}^{n-1}(2^j - 1) + \frac{1}{2}(2^n - 1)\right]$	$2l_m\theta_{y1'}\sum_{j=1}^{n-1}(2^j - 1)$

performing the indicated sums

$$\Delta x = 2l_m\theta_{x1}(\tfrac{3}{2}\,2^n - n - \tfrac{3}{2})$$

$$\Delta y = 2l_m\theta_{y1}(2^n - n - 1).$$

For large n ($n \gg 1$)

$$\Delta x \cong 2l_m\theta_{x1}2^n(\tfrac{3}{2})$$

$$\Delta y \cong 2l_m\theta_{y1}2^n.$$

the deflection axes x',y', and taking $b > d$, we see from Fig. 17(a) that a displacement of the beam $\Delta x'$ (or $\Delta y'$) produces a fractional loss of intensity

$$\frac{\Delta I}{I} = \frac{\Delta A}{A} \cong \frac{1}{\sqrt{2}}\left(\frac{1}{b} + \frac{1}{d}\right)\Delta x'(\text{or } \Delta y')$$

giving

$$\Delta x'(\text{or } \Delta y') \cong \sqrt{2}d\left(\frac{\Delta I}{I}\right). \tag{70}$$

The diffraction angles θ_D for the x' and y' deflections are given by $\theta_{Dx'} = \sqrt{2}\lambda/b$ and $\theta_{Dy'} = \lambda/\sqrt{2}d$ as shown in Fig. 17(b). Combining these expressions with (68) and (69) we obtain,

$$\Delta x' = \beta_x l_m\left(\frac{\sqrt{2}\lambda}{b}\right)R_{x'} \leqq 0.2\sqrt{2}d \tag{71}$$

$$\Delta y' = \beta_y l_m\left(\frac{\lambda}{\sqrt{2}d}\right)R_{y'} \leqq 0.2\sqrt{2}d \tag{72}$$

for a fractional intensity loss of 20 percent. Combining (71) and (72)

we find

$$(R_{x'}R_{y'})^{\frac{1}{2}} \leqq \frac{0.2}{\sqrt{\beta_x\beta_y}\lambda}\left(\frac{bd}{l_m}\right)\sqrt{\frac{2d}{b}} \tag{73}$$

Substituting for $\mathcal{P}_r$ from (15) we obtain the desired result,

$$(R_{x'}R_{y'})^{\frac{1}{2}}\nu \leqq \Lambda_{x'x'}\mathcal{P}_r \tag{74}$$

where

$$\Lambda_{x'y'} = \frac{1}{5\alpha\sqrt{\beta_x\beta_y}\lambda\left[1+\frac{l_m-l}{l_m}\right]}\sqrt{\frac{2d}{b}} \ . \tag{75}$$

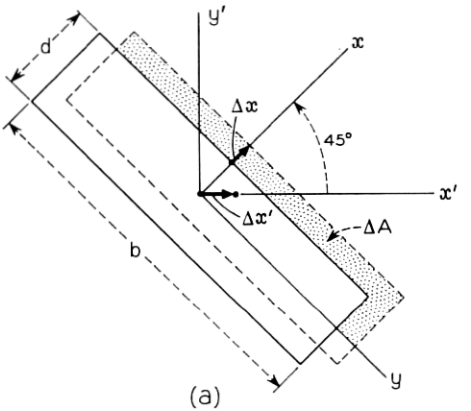

(a)

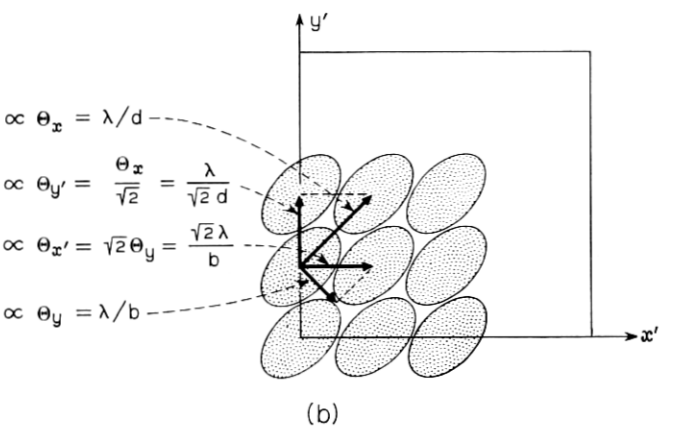

(b)

Fig. 17 — Rectangular aperture: (a) beam displacement, (b) image plane.

APPENDIX C

Dielectric Properties of KTN

From the Devonshire free energy expansion in (25) we can derive expressions for several useful dielectric properties. The spontaneous polarization P_s is given by

$$P_s = \sqrt{\frac{2}{3}} P_{so} \left[1 + \left\{ 1 + \frac{3}{4} \left(\frac{T_o - T}{T_c - T_o} \right) \right\}^{\frac{1}{2}} \right]^{\frac{1}{2}} \quad T < T_o \tag{76}$$

where P_{so} is the spontaneous polarization at the phase transition T_c, and is given by

$$P_{so} = \sqrt{\frac{-3\xi}{4\zeta}}. \tag{77}$$

The difference between the Curie Weiss temperature T_o and phase transition temperature T_c in the Devonshire model is,

$$T_c - T_o = \frac{3}{16} \epsilon_o C \left(\frac{\xi^2}{\zeta} \right). \tag{78}$$

The low field dielectric permittivity ϵ above the phase transition obeys a Curie-Weiss law,

$$\epsilon = \frac{C\epsilon_o}{T - T_o} \tag{79}$$

$$\lim_{\delta \to 0} \epsilon = \frac{C\epsilon_o}{T_c - T_o} \tag{80}$$

$$\delta \geqq 0$$

$$T = T_c + \delta$$

$$\lim_{\delta \to 0} \epsilon = \frac{C\epsilon_o}{4(T_c - T_o)} \tag{81}$$

$$\delta = \leqq 0$$

$$T = T_c + \delta .$$

More generally below T_o, the permittivity can be written

$$\epsilon_{T<T_c} = \frac{\epsilon_o C}{(T_c - T_o)\left[-\frac{4}{3} + \frac{16}{3}\gamma + \frac{20}{3}\gamma^2 \right] - (T_o - T)}, \tag{82}$$

where

$$\gamma \equiv \sqrt{1 + \frac{3}{4}\left(\frac{T_o - T}{T_c - T_o}\right)}. \tag{83}$$

The small signal permittivity at high fields is given by,

$$\epsilon_b \cong \frac{\epsilon}{1 + 3\epsilon\xi P_b^2 + 5\epsilon\zeta P_b^4}. \tag{84}$$

APPENDIX D

Power Considerations

Consider the circuit shown in Fig. 18. The current in the RF driver arm is given by

$$\begin{aligned} i_1 &= \frac{j\omega C_s V_{rf}}{\frac{C_s}{C_B} + j\omega C_s R_g + \left\{\frac{j\omega R_s C_s}{1 + j\omega C_s R_s + (R_s C_s / L_B)}\right\}} \\ &\cong \frac{\omega C_s V_{rf}(1 + jQ_s)}{Q_s} \end{aligned} \tag{85}$$

where $Q_s = \omega C_s R_s$ and the following inequalities are satisfied,

$$R_s, \omega L_B \gg \frac{1}{\omega C_s} \gg R_g, \frac{1}{\omega C_B}.$$

The instantaneous power delivered by the RF driver is,

$$\mathcal{P}_{\text{inst}}(\text{driver}) = \frac{\omega C_s V_{rf}^2}{2Q_s} + \frac{\omega C_s V_{rf}^2}{2Q_s}\cos 2\omega t - \frac{\omega C_s V_{rf}^2}{2}\sin 2\omega t. \tag{86}$$

In the same manner, we can obtain the instantaneous power delivered by the circuit to the modulator,

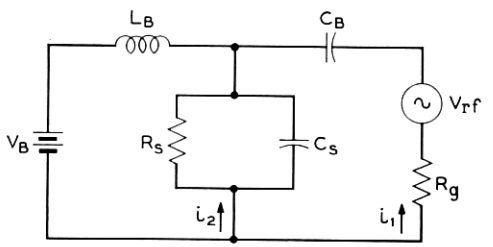

Fig. 18 — Equivalent circuit for biased operation.

$$\mathcal{P}_{\text{inst}}(\text{mod}) = \frac{V_B^2}{R_s} + \mathcal{P}_{\text{inst}}(\text{driver}) + \frac{2V_B V_{rf}}{R_s} \cdot \left(\cos \omega t - \frac{Q_s}{2} \sin \omega t\right). \tag{87}$$

The term V_B^2/R_s is supplied by the bias supply. It can be readily shown that the last term is supplied by the dc blocking capacitor and RF blocking inductor. The dc blocking capacitor contributes a term $(V_B V_{rf}/R_s)$ $(\cos \omega t - Q \sin \omega t)$ and the RF blocking inductor a term $(V_B V_{rf}/R_s)$ $\cos \omega t$. Since Q_s is large the instantaneous power delivered by the driver is to a good approximation given by,

$$\mathcal{P}_{\text{inst}}(\text{driver}) \cong \frac{\omega C_s V_{rf}^2}{2} \sin 2\omega t \tag{88}$$

the dissipated power in the modulator $(\langle \mathcal{P}_{\text{inst}(\text{mod})} \rangle_{\text{time}})$ from (87) is

$$\mathcal{P}_d = \frac{\omega C_s V_{rf}^2}{2Q_s} + \frac{V_B^2}{R_s}. \tag{89}$$

Since the actual modulation waveform is nonsinusoidal, the analysis must be extended to include a pulse-type waveform. In addition, since we are driving a reactive load we need to characterize the driver power requirements. The time average of the reactive power is zero. The peak instantaneous power depends on the risetime of the voltage pulse. Neither of these factors is a satisfactory measure of the required driver power. A more realistic quantity from the point of view of the driver[22] is the energy delivered to the modulator per address pulse times the number of address pulses/second. From the foregoing analysis, (88), the power defined in this fashion is given by

$$\mathcal{P}_r \equiv (\tfrac{1}{2} C V_{rf}^2) \nu_r, \tag{90}$$

where $\nu_r = 2\nu$ (assuming that each half cycle represents an addressing pulse). The dissipated power for the case of pulse modulation can be obtained from a simple extension of the foregoing analysis. Expanding the pulse waveform in a Fourier series,

$$v = \frac{4}{\pi} V_{rf} \sum_{m=1,3,5,\cdots} \frac{1}{m} \sin m\omega t$$

it is easily shown[23] that the power dissipated in the sample is given by

$$\mathcal{P}_d = \frac{16}{\pi^2} \left(\frac{\omega C_s V_{rf}^2}{2Q_s(\omega)}\right) \sum_{m=1,3,\cdots} \left(\frac{Q_s(\omega)}{mQ_s(m\omega)}\right). \tag{91}$$

If the quality factor Q_s is independent of frequency and the series is terminated at $m = 5$, (91) reduces to (29) of the text. The rise time of the pulse is approximately the rise time[24] associated with the highest frequency component $m_{max}\omega$

$$\tau_{rise} \cong \frac{0.45}{m_{max}\,\nu}. \tag{92}$$

It should be noted that the peak reactive power varies inversely with τ_{rise}, and can be substantially larger than the reactive power defined in (84) if the rise time is much shorter than the period of an address pulse.

The pulse amplitude has been equated to the half-wave voltage in the linear electro-optic modulator and to the incremental half-wave voltage in the biased quadratic modulator. This implies that an addressing pulse is needed for only one of the two polarization states of the light beam (i.e., either the "0" or "1" state but not both).

An alternative scheme is to set the ambient state of the modulator to a point midway between the two desired states ($\frac{1}{4}$ wave bias) in which case *each* state requires an address pulse of one half the previous amplitude. The average power required is thus cut by a factor of two. We have not used this latter scheme since in the case of KTN it introduces a possible dc component into the voltage across the modulator. In the case of the linear electro-optic materials the presently conceived[20] driver circuitry does not permit any increase in the available power using this bias scheme.

REFERENCES

1. Nelson, T. J., Digital Light Deflection, B.S.T.J., *43*, 1964, p. 821.
2. Tabor, W. J., Use of Wollaston Prisms for a High-Capacity Digital Light Deflector, B.S.T.J., *43*, 1964, p. 1153.
3. Chen, F. S., Geusic, J. E., Kurtz, S. K., Skinner, J. G., and Wemple, S. H., J. Apply. Phys., *37*, 1966, p. 388.
4. Nye, J. F., *Physical Properties of Crystals*, Oxford Univ. Press, 1960.
5. *American Institute of Physics Handbook*, McGraw-Hill Book Co. Inc., New York, 1963, Sect. 6, p. 188.
6. Sliker, T. R. and Jost, J. M., Appl. Phys. Lett., J. Opt. Soc. Am. *56*, 130 (1966).
7. Peterson, G. D., Ballman, A. A., Lenzo, P. V., and Bridenbaugh, P. M., Appl. Phys. Lett., *5*, 1964, p. 234.
8. Devonshire, A. F., Phil. Mag., *40*, 1949, p. 1040; *42*, 1951, p. 1065.
9. Tabor, W. J., A High-Capacity Digital Light Deflector Using Wollaston Prisms, B.S.T.J., (to be published).
10. Bonner, W. A., Dearborn, E. F., and Van Uitert, L. G., Bull. Am. Ceramic Soc., January, 1965.
11. Huffstuttler, M. C., Jr., Curran, R., and Barns, R. L., private communication.
12. Warter, P. J., Jr., private communication.
13. von Hippel, A., Gross, E. P., Jelatis, J. G., and Geller, M., Phys. Rev., *91*, 1953, p. 568.; Kurtz, S. K. and Warter, P. J., Jr. Bull. Am. Phys. Soc, *11*, p. 34(A) (1966).
14. Macdonald, J. R., J. Chem. Phys., *29*, 1958, p. 1346.
15. Rose, A. *Concepts in Photoconductivity and Allied Problems*, Interscience Pub., New York, 1963.

16. Kaminow, I. P., Appl. Phys. Lett., *7*, 1965, p. 123.
17. Johnson, A. R., Appl. Phys. Lett., *7*, 1965, p. 195.
18. Chen, F. S., private communication.
19. Ashkin, A., Boyd, G. D., Dziedzic, J. M., Smith, R. G., Ballman, A. A., Levinstein, J. J., and Nassau, K., Appl. Phys. Letters *9*, 1966, p. 72.
20. Turner, E. H., Appl. Phys. Lett., *8*, June, 1966; Lenzo, P. V., Spencer, E. G., and Nassau, K., J. Opt. Soc. Amer., *56*, 1966, p. 633.
21. Mason, W. P., *Piezoelectric Crystals and Their Applications to Ultrasonics*, D. Van Nostrand Co., New York, 1950, Chap. III, p. 61 and Chap. XII, p. 303.
22. Petersen, R. C., private communication.
23. Lawrence, R. R., *Principles of Alternating Currents*, McGraw-Hill Book Co. Inc., New York, 1935, Chap. III, p. 94.
24. Lewis, I. A. D. and Well, F. H., *Millimicrosecond Pulse Techniques*, Pergamon Press, 2nd Ed., London, 1959, Chap. I, p. 7.